PROCEEDINGS OF THE 2nd WORKSHOP ON POSITIONING, NAVIGATION AND COMMUNICATION (WPNC'05)
& 1st ULTRA-WIDEBAND EXPERT TALK (UET'05)

Low cost resolution enhancement in hyperbolic localization

Holger Linde, Edwin Naroska[a], Guido Stromberg[b]

[a]Computer Engineering Institute, University Dortmund, Germany,
Email: Holger.Linde@udo.edu
[b]Infineon Technologies, Munich, Germany

Abstract - Providing physical position information of humans and objects is one of the key issues for location and context aware applications in pervasive computing. A common approach for location estimation is hyperbolic localization. Following this method, time difference of arrival (TDOA) measurements among a mobile and fixed reference units are performed. For this purpose, these units are equipped with clocks which must be synchronized among each other. This is particularly critical when electromagnetic waves are used which propagate at the speed of light. In this case clocks must operate at a very high precision and are therefore complex and expensive. Furthermore they are difficult to synchronize. We present a time acquisition approach for indoor hyperbolic localization using short pulse electromagnetic waves. Our method has two major advantages: a) A high location precision is obtained in spite of using relatively low frequency and unstable or drifting clock oscillators. This is achieved by transmitting bursts of pulses following a certain transmission pattern, and subsequent time averaging. As a consequence, localization equipment can be implemented in inexpensive standard CMOS without the need for sophisticated high speed circuitry. b) The participating units' clocks are implicitly synchronized which further reduces system complexity and cost. We provide simulation results that indicate how the achieved precision depends on various factors such as burst length and clock jitter.

1 Introduction

Hyperbolic localization has vastly been covered in literature for more than a decade (e.g. [7]). It is based on time difference of arrival measurements of signals transmitted among a mobile unit and a number of fixed reference units. The objective is the position estimation of the mobile unit. While TDOA ranging and localization applications have been developed using combined ultrasound and RF [11], combined acoustics and RF [5] and outdoor RF [3], indoor radio turned out to be difficult to utilize. One of the major issues in indoor position estimation using electromagnetic waves is multipath signal propagation. As a result, the original, direct line of sight signal transmitted by an RF unit is overlapped by multiple signal echos. For accurate time measurement it is therefore required to detect the leading edge of a received signal. A promising technology to do this is ultra wideband (UWB). Recently, UWB has gained attention among researchers as well as the communications and consumer industry [10]. Short pulse electromagnetics are especially suited for ranging as shown in [2]. In [4] a commercial UWB based localization system is presented. Experiments were made in a severe multipath shipboard environment. Results show that UWB is well suited for ranging even under tough conditions.

The principle setup for hyperbolic localization in the plane is shown in Fig. 1. At least three fixed reference units a, b and c are deployed in the environment. m is the mobile unit

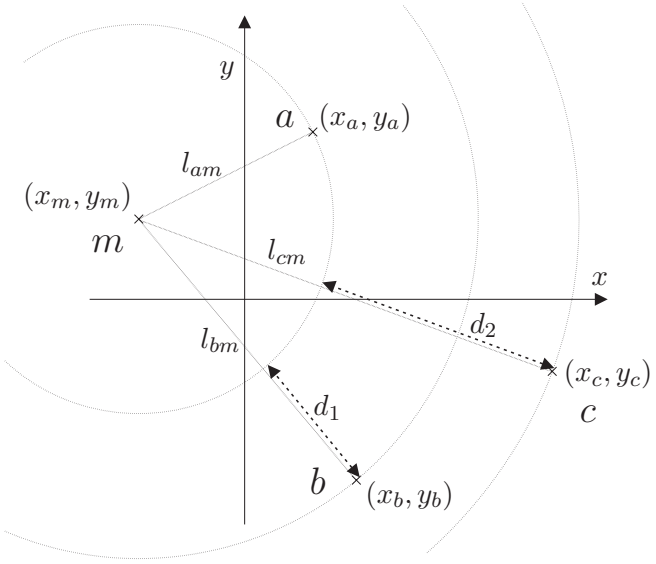

Figure 1: Localization based on distance differences

that is to be localized. A signal emitted by m is received by the reference units after time spans corresponding to their respective physical distances from m. In general, distances between units p and q are denoted l_{pq}, with $p, q \in \{a, b, c, m\}$). For location estimation, two TDOA measurements are considered which yield the distance differences $d_1 = l_{am} - l_{bm}$ and $d_2 = l_{am} - l_{cm}$. Typically, for time measurements a clock is needed on each of the reference units as well as the mobile unit. Furthermore, the reference units' clocks must be synchronized in order to determine the time span between two signal reception times. In case of radio signals, synchronization of the clocks is critical: even a small synchronization deviation may result in huge measurement errors. This problem is addressed in [9], where a hyperbolic localization approach using implicit clock synchronization is described. Synchronization is achieved by adding TDOA reference measurements among the reference units that are performed shortly before or after the actual localization measurement. With this addition, the measurement procedure looks like this:

- Localization measurement
  A signal is emitted by m. On reception of this signal a, b and c take a snapshot of their internal clocks.

- Reference measurements
  In order to synchronize the reference units' clocks implicitely, b resp. c act as a sender and the remaining reference units as receivers. Exploiting the geometrical arrangement, all timing offsets can be eliminated.

- From these three measurements, the distance differences d_1 and d_2 can be determined and thus the position (x_m, y_m) of the mobile unit.

Here, we extend this concept by integrating quartz oscillators and digital counters for time measurement. In order to measure time spans with a precision sufficient to resolve distances in the range of centimeters, highly accurate very high frequency clocks are required at the reference units. Unfortunately, this conflicts with the need to make the entire localization equipment as cheap as possible. In this paper, we show that low clock frequencies in the order of 100 MHz are sufficient to obtain a location precision in the range of a few centimeters. Short term instabilities of the oscillators are taken into account and analyzed. Middle and long term drift caused

by varying ambient conditions and aging are compensated by following a certain transmission pattern.

2 Resolution enhancement by time averaging

In order to enhance the precision of the clocks embedded in the reference stations, the TDOA measuring procedure described above is modified as follows.

- As stated above, instead of a single pulse a transmitter station p now emits a contiguous train of N pulses with constant frequency $1/T_p$ (see Fig. 2). The transmitter is resetted at $t_p = 0$. After a delay of $t_{s0,p}$, emission of pulses is initiated. The resulting signal is denoted s_p.

- The reference nodes sample the received signal s_q using a (relatively) low frequency clock which runs at $1/T_q$ (with T_q being the clock period at reference unit q). Furthermore, with each clock tick of T_q a counter C_q is incremented by one.

  If a newly sampled value is equal to 1 while the preceding sampled value was 0, the current counter value $C_{q,i}$ is added to a sum S'_q, with $i \in \{0, 1 \ldots N-1\}$. E.g., in the example shown in Fig. 2 the counter values $C_{q,0} = 5$ and $C_{q,1} = 8$ are added. The sum is initialized to 0 before the measurement begins. The process continues until N counter values have been added to S'_q.

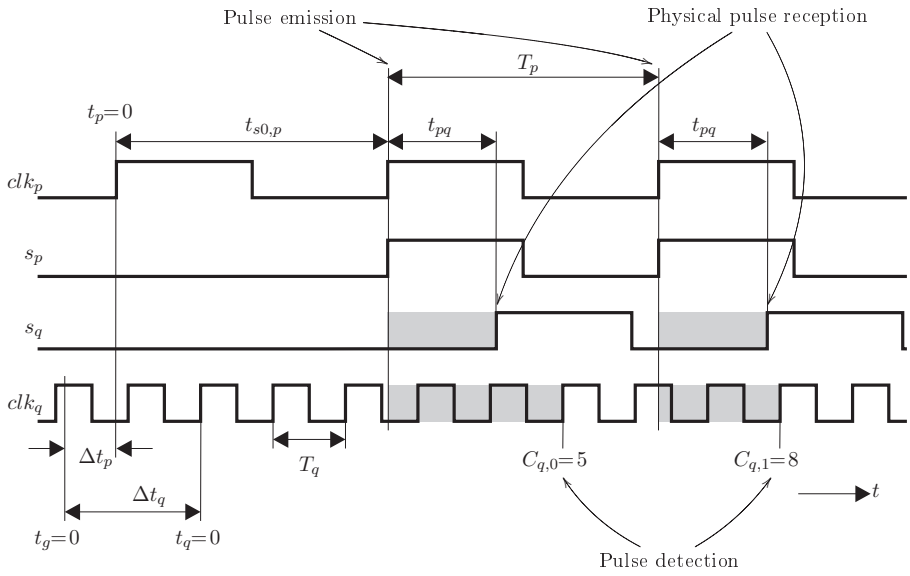

Figure 2: Pulse transmission clock scheme

The time value S_q corresponding to the sum S'_q can be obtained as follows:

$$S_q = T_q \cdot S'_q = T_q \cdot \sum_{i=0}^{N-1} C_{q,i},$$

where $C_{q,i}$ represents the counter value after the $(i+1)$-th detection of a rising edge of s_q. Note that the start value of the counter is nonrelevant as long as the counter does not overflow during

operation. I.e., it can be reseted after the N-th sample. $C_{q,i}$ can be replaced such that

$$S_q = \sum_{i=0}^{N-1} T_q \lceil \frac{i \cdot T_p + t_{pq} + t_{s0,p} + \Delta t_p - \Delta t_q}{T_q} \rceil, \tag{1}$$

where t_{pq} is the time of flight of the signal from station p to station q. Δt_p and Δt_q are the clock offsets of the station p and q to a *virtual* global clock t_g, such that

$$t_g = t_p + \Delta t_p.$$

The physical propagation time t_{pq} is what we are actually looking for while all other parameters are given or eliminated by the reference measurements as described in [9]. Unfortunately, t_{pq} is argument to a ceiling function in (1) and hence cannot be directly extracted from the equation. However, for sufficiently deviant transmitter and receiver clock frequencies, S_q can be rewritten as

$$S_q = \sum_{i=0}^{N-1} \left(i \cdot T_p + t_{pq} + t_{s0,p} + \Delta t_p - \Delta t_q + \Phi \right),$$

where Φ represents a random process that generates equally distributed real numbers from the interval $[0, T_q)$. In the next step, the average is determined by dividing by N. The result is described by the central limit theorem: $\hat{S}_q$ in turn is a random variable that is normally distributed (indicated by $\mathcal{N}$) with mean value μ and variance σ^2[1]:

$$\hat{S}_q \sim \mathcal{N}\left(\mu = t_{pq} + t_{s0,p} + \Delta t_p - \Delta t_q + \frac{(N-1)T_p + T_q}{2}, \quad \sigma^2 = \frac{{T_q}^2}{12N} \right) \tag{2}$$

As a result, in comparison to a single measurement, the standard deviation σ of the random process $\hat{S}_q$ decreases by $\sqrt{N}$. I.e., the measurement precision can be improved by increasing N.

Oscillator considerations

In the ideal case, the clocks T_p and T_q are running at a constant fixed frequency. Our aim is to use inexpensive COTS (commericial off-the-shelf) quartz clock oscillators for time measurements and general operation of the participating nodes. In our application, we must consider frequency and phase stability issues. Typically, these effects can be divided in long and short term influences[6]:

- Long term frequency stability is affected by device aging due to internal changes in the oscillator, e.g. the relaxation of stresses. As a result, its frequency will slowly drift from the nominal value. Typical values for aging are 3 ppm (parts per million) in the first year and 1 ppm/ yr beyond. In Sec. 3 we discuss how long term bias can be compensated.

- Short term stability is affected by operating temperature, variation of supply voltage, load condition, shock and vibration. Typical values for commercial devices are 10 . . . 100 ppm. Phase and amplitude noise as a result of these effects lead to different sorts of jitter (see Sec. 2). A common definition of jitter can be found in [8]: "*The deviation from the ideal timing of an event.* [. . .] *Jitter is composed of both deterministic and Gaussian (random) content.*"

Clock jitter

Deterministic jitter of clock signals has a non-Gaussian probability density function and is always bounded in amplitude. It is caused by crosstalk effects from EMI sources (adjacent lines,

power supply noise, etc.). Since these error sources are implementation dependant, we neglect deterministic jitter in our model.

Random jitter is characterized by a Gaussian distribution. It is caused by a number of stochastic processes including thermal vibrations. The most common jitter measure is period jitter (see Fig. 3).

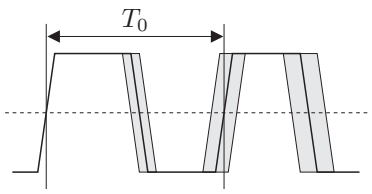

Figure 3: Period jitter

It is the time difference between a measured cycle period and the ideal cycle period T_0 and is given as either peak-to-peak or root mean square (RMS). For typical crystal clocks, the period jitter may range from 5 to 50 ps RMS. As we are actually interested in achieving a precision of the same order as these values (a propagation time of 50 ps corresponds to a 15 mm distance in air), clock jitter must be taken into account. Accumulated random jitter is unbounded and can therefore severely affect the measurement precision of the system.

To account for the effect of clock jitter z on $\hat{S}_q$ we model the clock jitter as white gaussian noise

$$z \sim \mathcal{N}(\mu_z = 0, \quad {\sigma_z}^2 = {\sigma_p}^2 + {\sigma_q}^2),$$

where σ_p and σ_q are the standard deviations of the sender clock of node p and the receiver clock of node q, resp. Note that this model requires that N does not become too big. Otherwise, the accumulated jitter will cause a significant phase shift of the clocks.

Calculating $\hat{S}$- differences

Actually, we are not interested in the mean value of $\hat{S}_q$. Instead, we determine the difference of $\hat{S}$ values of two receivers q and r, since they yield the time differences of arrival. Calculating $\hat{S}_q - \hat{S}_r$ yields

$$\hat{S}_q - \hat{S}_r \sim \mathcal{N}\left(\mu = t_{pq} - t_{pr} + \Delta t_r - \Delta t_q + \frac{T_q - T_r}{2}, \quad \sigma^2 = \frac{T_q^2 + T_r^2}{12N} + \frac{2\sigma_z^2}{N}\right),$$

i.e., the standard deviation decreases by $1/\sqrt{N}$. Note that $\Delta t_r - \Delta t_q$ can be eliminated by the reference measurements described in [9]. Hence, $t_{pq} - t_{pr}$, a term proportional to a distance difference shown in Fig. 1, can finally be obtained. E.g., $t_{ma} - t_{mb}$ yields d_1.

3 Simulation results

We have designed a simulation model of the localization system based on the time averaging approach described above. We have implemented the model using VHDL. In the first set of simulations, we have evaluated how fast the measurement errors Δd_1 and Δd_2 decline, depending on various device configurations of clock frequencies and jitter. Data aquisition was done following a certain pattern, shown in Fig. 4(a). The grey boxes represent time slots in which the actual measurements are performed, as depicted in Fig. 2. We refer to one such slot as transmission mode b, c or m. The measurement procedure is therefore:

- b is sender, a and c are receivers. N_b measurements are taken and averaged.
- c is sender, a and b are receivers. N_c measurements are taken and averaged.
- m is sender, a, b and c are receivers. N_m measurements are taken and averaged.

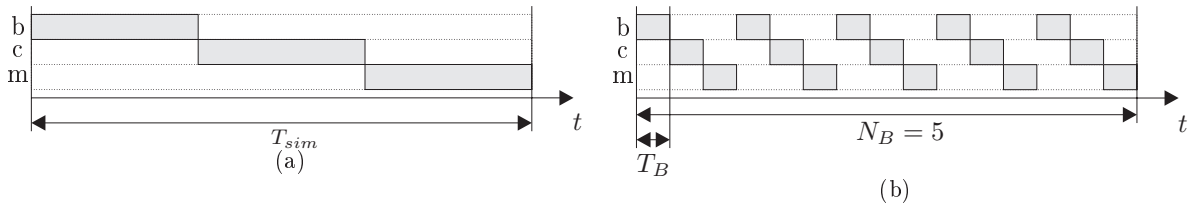

Figure 4: Transmission patterns for one-time (a) and multiple (periodic) (b) synchronization

- d_1 and d_2 are computed according to [9].

Fig. 5 shows measurement errors against measurement time for various device configurations. Without jitter and very similar clock frequencies, an error of below 0.5 m can be achieved instantly (a). Simulation results (b) and (c) show that more deviant clock frequencies holding the same period jitter can support the system in that the error converges faster. It can also be seen that due to jitter, precision cannot infinitely be increased.

Periodic resynchronization

As indicated above, accumulated jitter can corrupt the entire measurement: once the receiver clock phase (as a result of accumulated jitter) has shifted by a certain amount, not only the *current* but also *all subsequent* measurements will be affected. As a consequence, the overall result is heavily biased. This implication can be limited by periodic resynchronization: instead of one long burst of measurements, many smaller bursts are performed. Every time all modes have been passed through, the system has been implicitly resynchronized. Hence, jitter cannot grow unboundedly. This modified pattern is shown for $N_B = 5$ burst cycles in Fig. 4(b). The time span of one burst is denoted T_B. Instead *one* data set of size N_b, N_c and N_m, resp., *multiple* data sets of size $N_{b,i}$, $N_{c,i}$, and $N_{m,i}$ are obtained, with $i \in \{1 \dots N_B\}$. These must simply be averaged again:

$$N_b = \sum_{i=1}^{N_B} N_{b,i}, \quad N_c = \sum_{i=1}^{N_B} N_{c,i}, \quad N_m = \sum_{i=1}^{N_B} N_{m,i}.$$

In practice, mode switches do not occur instantly, but are deferred for a certain time. We refer to this time span as *switch delay* t_{SD}. During this time, no measurements are performed. As a consequence, the more mode switches are accomplished, the less measurements will be performed in the overall simulation time. This context is depicted in Fig. 6: it shows the measurement error against the number of burst cycles for a system with 12 ps RMS clock jitter on all units, while the measurement time T_{sim} is constant. It can be seen that the error decreases when shortening burst cycles because of less jitter accumulation. Interestingly, this is true even though for less burst cycles, i.e. smaller N_B, a larger number of overall measurements N_b, N_c and N_m can be performed. This result is particularly important when stringent energy conditions must be met.

In the next set of simulations, we have examined the impact of different switch delays t_{SD} (5 µs and 50 µs) at different simulation times T_{sim} (60 ms and 6 ms), for various amounts of jitter. It can be seen that, shorter switching delays yield faster converging results since more mode switches can be performed in the same simulation time (Fig. 7(a),7(b)). However, with much less efforts (i.e. number of measurements) almost the same precision can be achieved in spite of a much shorter overall time (6 ms, Fig. 7(c)).

This – at first glance maybe contradicting – result puts up the question how far the number of measurements can be reduced without deteriorating the results. This question is examined in the next simulation, the results of which are shown in Fig. 8. Here, we simulated the same localization

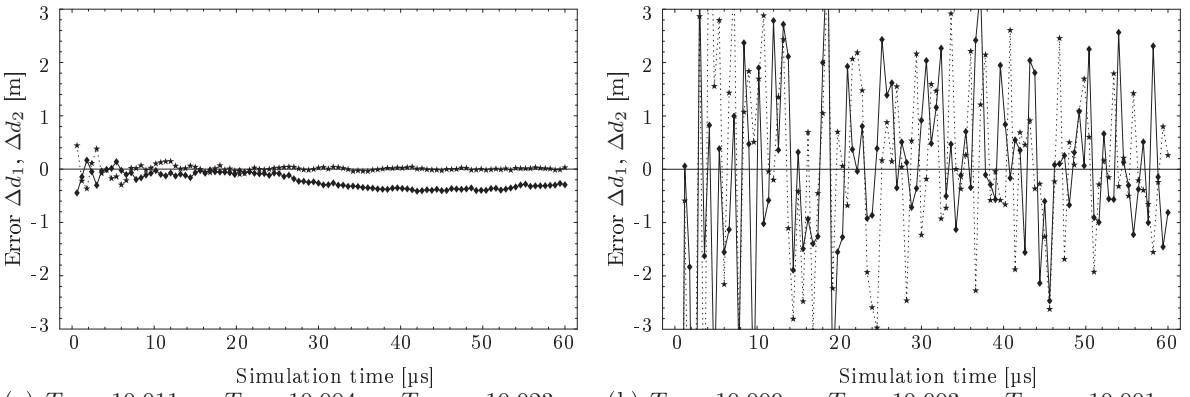

(a) $T_a = 10.011\,\text{ns}$, $T_b = 10.004\,\text{ns}$, $T_c = 10.023\,\text{ns}$, $T_m = 10.016\,\text{ns}$, no jitter

(b) $T_a = 10.009\,\text{ns}$, $T_b = 10.003\,\text{ns}$, $T_c = 10.001\,\text{ns}$, $T_m = 10.000\,\text{ns}$, 50 ps RMS jitter

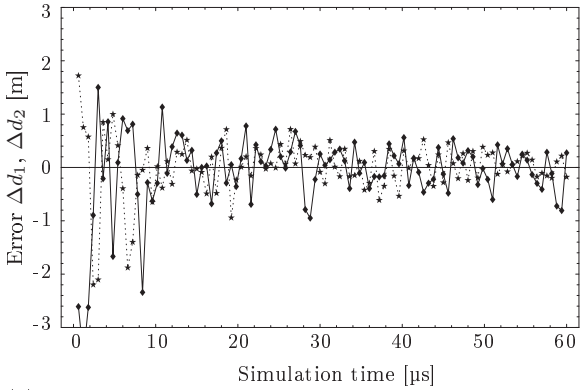

(c) $T_a = 10.777\,\text{ns}$, $T_b = 10.417\,\text{ns}$, $T_c = 10.309\,\text{ns}$, $T_m = 10.000\,\text{ns}$, 50 ps RMS jitter

Figure 5: Measurement errors Δd_1 and Δd_2 (dashed) against measurement time, without periodic clock synchronization

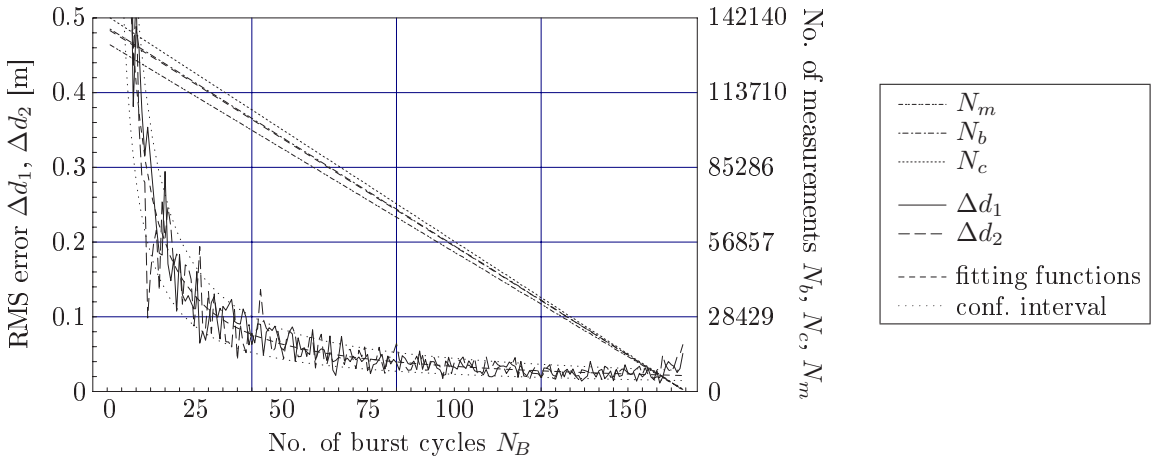

Figure 6: Measurement error against no. of burst cycles, with constant overall measurement time $T_{sim} = 50\,\text{ms}$ and switch delay $t_{SD} = 50\,\mu\text{s}$

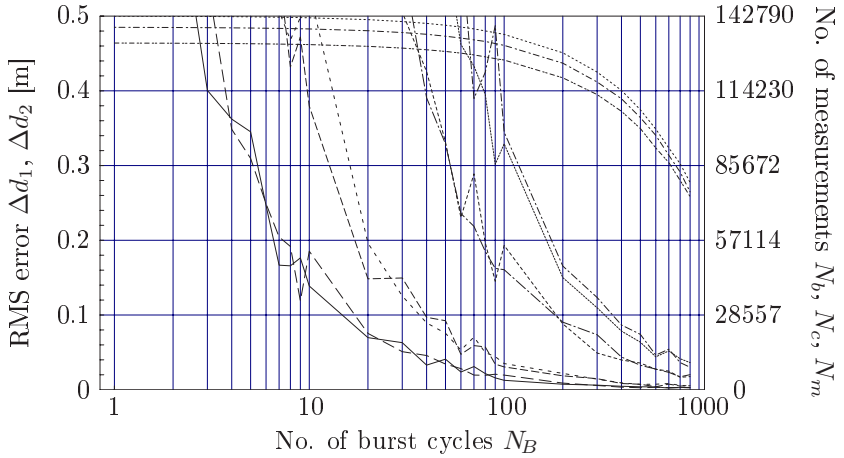

(a) $t_{SD} = 5\,\mu s$, $T_{sim} = 60\,ms$

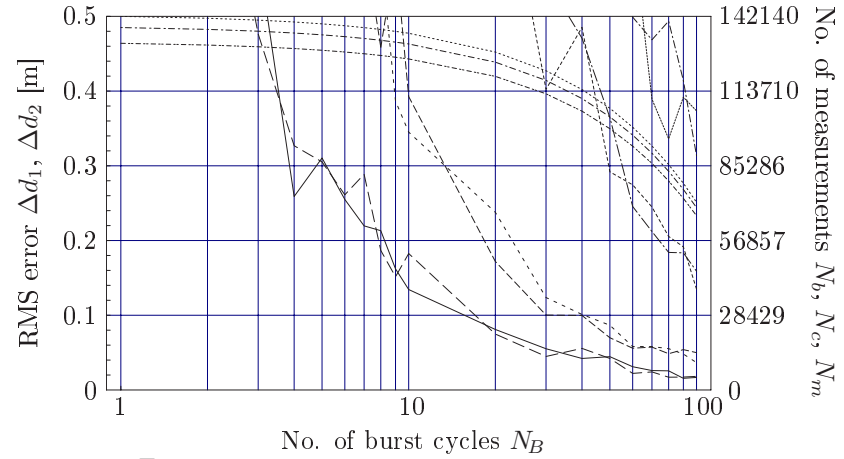

(b) $t_{SD} = 50\,\mu s$, $T_{sim} = 60\,ms$

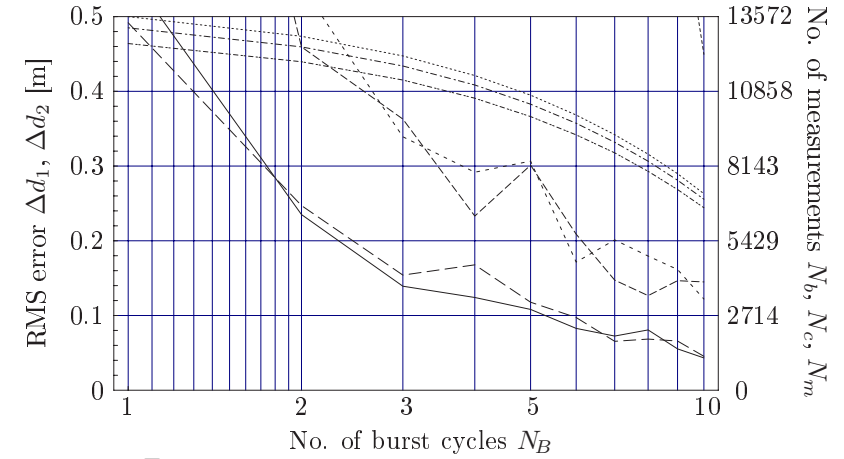

(c) $t_{SD} = 50\,\mu s$, $T_{sim} = 6\,ms$

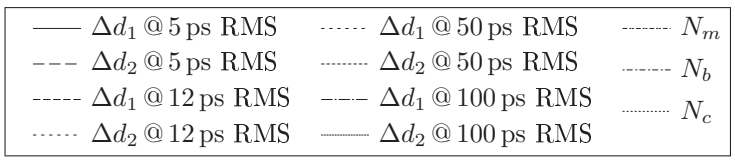

Figure 7: Measurement error against number of burst cycles for various device configurations and different amounts of jitter

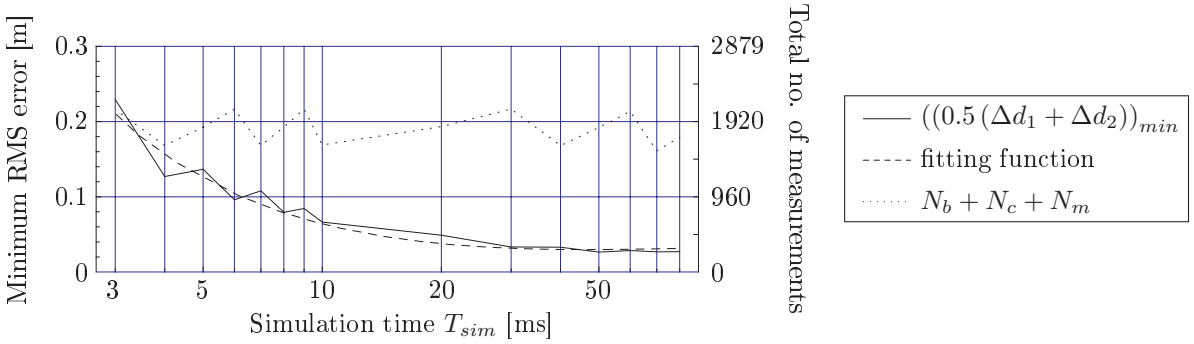

Figure 8: Measurement error against simulation time, $t_{SD} = 50\,\mu s$

system as in Fig. 6, for simulation times from 3 to 80 ms. For each simulation, a fitting function for the average standard error as well as a confidence interval (the width of which was chosen according to the number of simulations that were run to compute statistics) was determined. Furthermore, for each simulation, the minimum of the upper bound of this interval was chosen as the upper error limit, and the corresponding number of measurements and transmission pattern were noted down. This plot therefore represents the maximum precision that can be achieved for a certain simulation time. Interestingly, for all T_{sim} in this setup, similar efforts, i.e. number of measurements, must be done.

Frequency bias compensation

To compensate long term frequency biases of all participating units, only one of them need be equipped with a long term stable oscillator. From this oscillator, the other devices can derive clock correction factors s_p for their own clocks. For this purpose, we add an additional full measurement, such that four reference measurements (two where b resp. c is the sender) and two localization measurements (where m is the sender) are performed. This scheme ist illustrated in Fig. 9.

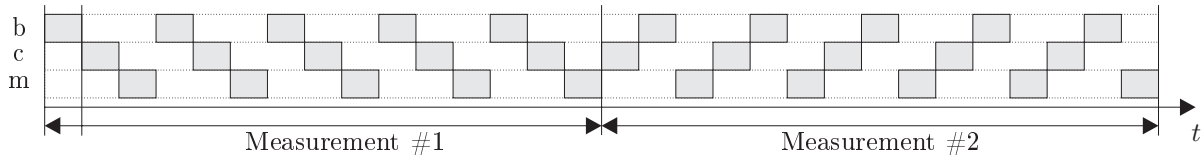

Figure 9: Advanced transmission pattern with high jitter resistance and additional full measurement to compensate long term clock drift

For proper operation, after production of each device the exact clock period $T_{p,0}$ of its oscillator must once be measured. Then, during operation, the current clock period T_p can be computed by

$$T_p = T_{p,0} \cdot s_p, \quad p \in \{a, b, c, m\}.$$

s_p is the frequency bias compensation factor and is very close to 1. When two full measurements are performed, two sets of distance differences $\hat{d}_1, \hat{d}_2$ (for measurement #1) and $\hat{d}'_1, \hat{d}'_2$ (for measurement #2) are determined. With $\hat{d}_1 = \hat{d}'_1$ and $\hat{d}_2 = \hat{d}'_2$, the compensation factors s_b and s_c can be found if s_a is known (in this case, a is the device with a highly stable clock):

$$s_b = f(s_a), \quad s_c = f(s_a)$$

Finally, all T_p in the equations of the previous chapter must be substituted by $T_{p,0} \cdot s_p$.

4 Conclusion

We have presented a time measurement approach for RF based hyperbolic indoor localization using inexpensive low frequency oscillators. By means of time averaged pulse bursts we achieve a timing resolution far below the oscillators' clock period. Clocks are implicitly synchronized during the localization procedure. Long term clock drifts can be compensated. The impact of short term effects (jitter) can be restricted by choosing an appropriate transmission pattern. Long term clock drifts caused by e.g. device aging can be compensated. This approach is particularly promising for indoor localization using UWB.

References

[1] I. N. Bronshtein, K. A. Smendyayev, G. Musiol, and H. Muehlig. *Handbook of Mathematics*. Springer, Berlin, 2004.

[2] W. C. Chung and D. S. Ha. An accurate ultra wideband (UWB) ranging for precision asset location. In *IEEE Conference on Ultra Wideband Systems and Technologies (UWBST)*, pages 389–393, Reston, VA, USA, November 2003.

[3] A. Dersan and Y. Tanik. Passive radar localization by time difference of arrival. In *Military Communications Conference (MILCOM)*, pages 1251–1257, Anaheim, CA, USA, October 2002.

[4] R. J. Fontana. Experimental results from an ultra wideband precision geolocation system. In *Ultra-Wideband, Short-Pulse Electromagnetics 5*, pages 215–224. Kluwer, NY, 2000.

[5] L. Girod and D. Estrin. Robust range estimation using acoustic and multimodal sensing. In *IEEE Intelligent Robots and Systems (IROS)*, volume 3, pages 1312–1320, Maui, HI, USA, November 2001.

[6] Hewlett-Packard. Fundamentals of Quartz Oscillators, Application Note 200-2, 1997.

[7] K. C. Ho and Y. T. Chan. Solution and performance analysis of geolocation by TDOA. *IEEE Transactions on Aerospace and Electronic Systems*, 29(4):1311–1322, October 1993.

[8] Fibre Channel – Methodologies for Jitter Specification, T11.2/Project 1230/ Rev 10, June 9, 1999.

[9] H. Linde, E. Naroska, G. Stromberg, and T. Sturm. TDOA localization using implicit clock synchronization. In *13th IST Mobile and Wireless Communications Summit*, volume 2, pages 722–726, Lyon, France, June 2004.

[10] I. Oppermann, M. Hämäläinen, and J. Iinatti. *UWB – Theory and Applications*. Wiley, 2004.

[11] N. B. Priyantha, A. Chakraborty, and H. Balakrishnan. The cricket location-support system. In *6th International Conference on Mobile Computing and Networking (MobiCom)*, pages 32–43, Boston, MA, USA, August 2000.